

# Incorporating NDVI-Derived LAI into the Climate Version of RAMS and Its Impact on Regional Climate

LIXIN LU

*Department of Hydrology and Water Resources, The University of Arizona, Tucson, Arizona, and Department of Atmospheric Science, Colorado State University, Fort Collins, Colorado*

W. JAMES SHUTTLEWORTH

*Department of Hydrology and Water Resources, The University of Arizona, Tucson, Arizona*

(Manuscript received 7 February 2001, in final form 8 December 2001)

## ABSTRACT

In this study, a climate version of the Regional Atmospheric Modeling System (ClimRAMS) was used to investigate the sensitivity of regional climate simulations to changes in vegetation distribution in the Great Plains and Rocky Mountain regions of the United States. The evolution of vegetation phenology was assimilated into the ClimRAMS in the form of estimates of the leaf area index (LAI) derived from the normalized difference vegetation index (NDVI). Initially, two model integrations were made. In the first, the NDVI-derived vegetation distribution was used, while the second integration used the model's "default" description of vegetation. The simulated near-surface climate was drastically altered by the introduction of NDVI-derived LAI, especially in the growing season, with the run in which observed LAI was assimilated producing, in general, a wetter and colder near-surface climate than the default run. A third model experiment was then carried out in which the (comparatively more homogeneous) spatial distribution of the LAI remained the same as in the "default" run, but the overall, domain-averaged magnitude of the LAI was reduced to be consistent with that of NDVI-derived LAI. This third run simulated a drier and warmer near-surface climate compared to the default run. Taken together, these results indicate that regional climates are indeed sensitive to seasonal changes in vegetation phenology, and that they are especially sensitive to the land surface heterogeneity associated with vegetation cover. The need to realistically represent both the spatial and temporal distribution of vegetation in regional climate models is thus highlighted, and the value of assimilating remotely sensed measures of vegetation vigor in Four-Dimensional Data Assimilation (4DDA) systems is demonstrated.

## 1. Introduction

Most land surfaces are covered by vegetation, and there is general recognition of the importance of vegetation control on the exchange of energy, mass, and momentum between the land surface and the atmosphere. For example, Gash and Nobre (1997) reviewed the climatological measurements from the Anglo-Brazilian Amazonian Climate Observational Study (ABRACOS) and found that the difference in radiation and energy balance between forests and clearings produces higher air temperatures in the clearings, particularly in the dry season. In areas of substantial deforestation, higher sensible heat fluxes from the cleared forests produce deeper convective boundary layers, with differences in cloud cover being observed and mesoscale circulations predicted. Based on low-level flight measure-

ments, Segal (1989) showed that the atmospheric boundary layer is shallower, cooler, moister, and less turbulent over irrigated cropland than over adjacent bare soil surfaces. Similarly, an observational study conducted by Rabin et al. (1990) showed that convective clouds are first formed over a harvested wheat field surrounded by growing vegetation and are suppressed immediately downstream of lakes and forests. In addition, Koster et al. (1986) indicated that the observed growing season precipitation peak may be due, in part, to the local recycling of water.

Climate model simulations have also shown significant sensitivities to land surface characteristics. Charney (1975) and Charney et al. (1977) demonstrated that such models are sensitive to gross, global-scale changes in specified surface albedo (a 5% increase in albedo led to a precipitation reduction of 5%–20%). However, changes in soil moisture, roughness length, and soil and vegetation characteristics have also been shown to have at least comparable effects (Shukla and Mintz 1982; Sud and Smith 1985; Meehl and Washington 1988). Chase

---

*Corresponding author address:* Dr. W. James Shuttleworth, Dept. of Hydrology and Water Resources, The University of Arizona, Tucson, AZ 85721.  
E-mail: shuttle@hwr.arizona.edu

et al. (1996) examined the sensitivity of a general circulation model (GCM) to global changes in leaf area index (LAI) and found that decreasing LAI globally decreased the surface latent heat flux and increased the sensible heat flux during January and July. More recently, Chase et al. (2000) showed that regional landscape changes in the Tropics alter climate, not only regionally but also globally, by modifying the position and intensity of the mid- and high-latitude polar jet stream through teleconnections. Copeland et al. (1996) used a regional climate version of the Regional Atmospheric Modeling System (RAMS) to assess the impact of a natural versus the current vegetation distribution on the weather and climate. The resulting simulated changes in meteorological variables at screen height were closely related to changes in vegetation parameters, specifically to the albedo, roughness length, LAI, and fractional vegetation cover. Pielke et al. (1997) demonstrated the significant role that land-use change has in generating thunderstorms. Using the National Center for Atmospheric Research (NCAR) Regional Climate Model (RegCM), Bonan (1997) studied the effects of land-use change on the climate of the United States. His results suggested that the replacement of the natural vegetation by present-day vegetation cover over the United States has caused a cooling of 1 K over the eastern part of the country and a warming of 1 K over the western part during spring. His simulations also showed a warming of about 2 K during the summer over large regions of the central United States.

The seasonal cycle and interannual variation of vegetation also exerts a significant control on surface-atmosphere interactions. Dirmeyer (1994), for instance, showed that the inclusion of dormant vegetation during the spring and early summer in a GCM run greatly reduces surface moisture fluxes by eliminating transpiration from leaves, and prevents further depletion of moisture in the root zone of soil, leading to soil-moisture recovery during the subsequent summer. Xue (1997) investigated the impact of land surface degradation in the Sahel on seasonal variations of atmospheric and hydrological components over tropical North Africa using a GCM. He found that desertification increases the surface air temperature and reduces precipitation, runoff, and soil moisture over the Sahel region during the summer months. This impact is not limited to the desertified area but also propagates to the south and extends into winter months. Another study, conducted by Xue et al. (1996) using the Center for Ocean-Land-Atmosphere Studies (COLA) GCM, found that the erroneous prescription of crop vegetation phenology in the surface model contributed greatly to the temperature biases of summer simulation in the United States.

Bounoua et al. (2000) examined the sensitivity of a coupled atmosphere-biosphere GCM to changes in vegetation density and found that increasing vegetation density globally caused both evapotranspiration and precipitation to increase. Their results showed a cooling of

about 1.8 K in northern latitudes during the growing season and a slight warming during the winter, but with a year-round cooling of 0.8 K in the Tropics. Much recent work (e.g., Claussen 1994, 1998; Foley 1994; Texier et al. 1997; Claussen et al. 1998; Pielke et al. 1999) has shown that the initial specification of the land surface exerts a strong control on the subsequent atmospheric circulation in global and regional climate prediction models. A previous study by one of the authors using the coupled atmosphere and ecosystem model, RAMS-CENTURY (Lu et al. 2001), also showed that not only the initiation but also the variation in vegetation phenology and its associated land surface heterogeneity play a sizeable role in surface energy partitions and influence predictions of surface temperature and precipitation.

Advances in satellite remote sensing technology have provided unprecedented observations valuable for earth science study. The remotely sensed normalized difference vegetation index (NDVI) yields information on the spatial and temporal distribution of vegetation at regional and global scales. Oleson and Bonan (2000) studied the effect of remotely sensed plant functional type and LAI on the simulation of surface fluxes for boreal forest using the NCAR land surface model and found a substantial modeled response to spatial heterogeneity. Oleson et al. (2000) evaluated land surface parameters in the Biosphere-Atmosphere Transfer Scheme (BATS) using data from the International Satellite Land Surface Climatology Project Initiative 1 (ISLSCP-1) and Pathfinder Advanced Very High Resolution Radiometer (AVHRR) data. They found that land cover heterogeneity within grid cells and, for a given land cover type, leaf area index were much more spatially variable than assumed in BATS in 1988 and 1993, particularly in summer months. They suggested that improved parameterizations are needed in BATS to recognize the spatial variability in LAI and roughness length, as well as in their interannual variability. Whether remotely sensed data can improve the simulation of weather and climate is a question that can only be answered by incorporating relevant data into models and performing coupled simulations.

The majority of previous studies have focused on appraising impacts of assimilating observed vegetation density into GCMs or stand-alone land surface models. In the current study, we use Colorado State University's RAMS to examine the sensitivity of simulated regional climate to multiyear satellite observations of vegetation changes (NDVI). In its current form, RAMS land-surface hydrological processes (e.g., evaporation and transpiration), energy exchanges (e.g., latent heat and sensible heat fluxes), momentum exchanges (e.g., roughness length), and biophysical parameters (e.g., vegetation albedo, transmissivity, and stomatal conductance) are parameterized to have a strong dependence on the value of LAI. Consequently, inadequate and unrealistic description of the vegetation distribution and its evo-

TABLE 1. Model options used in the present study.

Category	Options selected	References
Basic equations	Nonhydrostatic; compressible	Tripoli and Cotton (1980)
Vertical coordinates	Terrain-following sigma z	Clark (1977), Tripoli and Cotton (1982)
Horizontal coordinates	Oblique polar-stereographic projection	
Grid stagger and structure	Arakawa C grid, multiple nested	Arakawa and Lamb (1977) grids (fixed)
Time differencing	Hybrid	
Large-scale precipitation	Dump-bucket	Cotton et al. (1995), Rhea (1978)
Convective parameterization	Modified-Kuo	Tremback (1990)
Radiation	Mahrer/Pielke	Mahrer and Pielke (1977)
Cloud	Thompson	Thompson (1993)
Surface layer	Louis Prognostic soil model Vegetation parameterization	Louis (1979), Louis et al. (1982) Tremback and Kessler (1985) McCumber and Pielke (1981), Avissar and Mahrer (1988), Lee (1992)

lution in the current RAMS land-surface models is considered a major deficiency. Using NDVI datasets to derive LAI can provide a more realistic vegetation distribution, which has the potential of improving the regional climate model simulations. The goal of the present study was to gain insight into the likely impact of directly assimilating NDVI-derived-LAI specification on the near-surface climate variables modeled by RAMS at regional spatial scales and seasonal timescales.

The paper is organized as follows. The model description and grid configuration are described in section 2. In section 3, both the vegetation and meteorological observational datasets used in this study are described, including their interrelationship. The NDVI-to-LAI conversion algorithm adopted for this study is also explained in this section. In section 4, the experimental design and the impact of vegetation on the simulated regional climate are examined. Discussion and conclusions are given in section 5.

## 2. Model description and control run design

### a. Climate version of RAMS

RAMS is a three-dimensional, nonhydrostatic, general purpose atmospheric simulation modeling system consisting of equations of motion, heat, moisture, and mass continuity in a terrain-following coordinate system (Pielke et al. 1992). The climate version of RAMS (ClimRAMS), which is a substantial modification of the original RAMS model (Liston and Pielke 2000), was used for this study. The model setup and options are very similar to those used by Lu et al. (2001) and are summarized in Table 1.

A prognostic soil and vegetation model that interacts with the modeled atmosphere provides the lower boundary condition in RAMS. Each grid cell is divided into three classes, which include open water, bare soil, and different types of vegetated surfaces. For bare soil, RAMS uses the multilayer soil model described by

Tremback and Kessler (1985). The moisture diffusivity, hydrologic conductivity, and moisture potential are as given by Clapp and Hornberger (1978). The thermal properties of the soil are a function of the soil moisture (Farouki 1986; Sepaskhah and Boersma 1979). The moisture at the deepest soil level is held constant through time, equal to the prescribed, initial value. The temperature of the bottom soil layer varies, following the deep-soil temperature model of Deardorff (1978). For the vegetated surface, RAMS uses the "big leaf" approach, with a layer of vegetation overlying a shaded soil (Avissar et al. 1985; Avissar and Mahrer 1988; Lee 1992) and 18 vegetation classifications, the parameters of each being defined based on BATS (Dickinson et al. 1981, 1993, 1998). The moisture extracted by transpiration from the soil is calculated by defining a vertical root profile (Dickinson et al. 1986) and removing water from the soil, depending on the fraction of roots in each soil layer. The surface-layer fluxes of heat, momentum, and water vapor are computed using the method of Louis (1979) and Louis et al. (1982). Vegetation leaf area index, fractional coverage, transmissivity, albedo, zero plane displacement height, and roughness length are needed as input to the land surface scheme in ClimRAMS in the form of regularly gridded space-time fields. In the current study, any grid cell with an estimated LAI value smaller than 0.1 units was treated as bare soil.

### b. Grid configuration and control run design

The model domain used in this study is shown in Fig. 1a. It comprises a coarse grid covering the entire conterminous United States at 200-km grid spacing and a finer, nested grid covering Kansas, Nebraska, South Dakota, Wyoming, and Colorado at 50-km grid spacing. The finer grid covers an area of 1500 km in the east-west direction and 1300 km in the north-south direction. The pole point for the oblique polar stereographic pro-

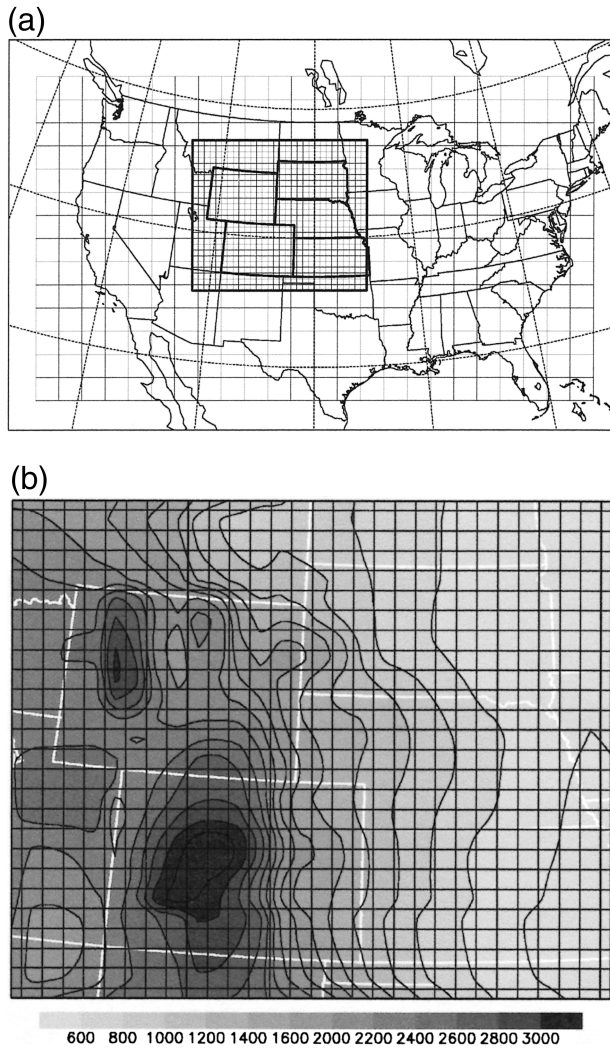


FIG. 1. (a) The simulation domain and grid configuration used for ClimRAMS in this study. The grid intervals used in the coarse- and fine-grid domains were 200 and 50 km, respectively. (b) The topographic distribution in m in the fine-grid domain.

jection used to define the grid is  $40^{\circ}\text{N}$ – $100^{\circ}\text{W}$ . There are 20 vertical levels in the modeled atmosphere, with a layer thickness of 119 m at the surface, stretching to 2000 m at the (23 km) top of the domain. The model is driven by 6-hourly lateral boundary conditions derived from National Centers for Environmental Prediction (NCEP) atmospheric reanalysis products (Kalnay et al. 1996). Lateral boundary condition nudging, which includes horizontal wind speed, relative humidity, air temperature, and geopotential height on pressure levels, is performed on the two outer-boundary grid cells of the coarse grid. The initial atmospheric fields are also provided from the NCEP reanalysis. The time step for the atmospheric model integrations is 2 min.

This domain has rather complex topographic features because it covers parts of the Great Plains and the Rocky Mountains (Fig. 1b). Heterogeneous soil types, based

on the U.S. Department of Agriculture (USDA) State Soil Geographic Database (STATSGO), were used within the model domain. (Miller and White 1998). The soil texture distribution for the finer grid is given in Fig. 2a. The model has 10 soil layers with boundaries at 2.0, 1.65, 1.3, 0.95, 0.65, 0.45, 0.3, 0.2, 0.125, and 0.05 m below the surface. The initial distribution of soil moisture is generated by first defining spatially constant soil-moisture content (i.e., 40% of the total water capacity) over the domain, and then running the model for 1 yr. The modeled soil-moisture distribution on the last day of that 1-yr simulation was then used as the initial condition for the next year's simulation.

The model vegetation distribution is defined using the International Geosphere–Biosphere Programme (IGBP) land-cover classification. Associated with this complex topography and soils, the domain also includes rather diverse vegetation classes, including C3 and C4 grassland, various agricultural croplands, evergreen needle-leaf trees, shrub land, and tundra. The distribution of the dominant vegetation cover in each element of the fine grid is shown in Fig. 2b. In fact, the inability to represent spatial heterogeneity within a given vegetation category is a significant deficiency of the standard RAMS classification. There is, for instance, no difference in this classification between grassland growing in northern Wyoming and that growing in southern Kansas, and these two regions will, unrealistically, have the same specification for LAI. When the LAI used in ClimRAMS is derived from remotely sensed NDVI, grassland vegetation in Wyoming can, and likely will, have a different LAI from that in Kansas because it is subject to different site-specific factors, not least the local climate. Similar differences will also apply to other vegetation classes. As a result, using remotely sensed LAI will inevitably introduce greater land-surface heterogeneity into the simulated domain.

### 3. Observational datasets

#### a. Vegetation observations

The Pathfinder AVHRR 10-day composite NDVI dataset for North America was used in this study. These data are available at 8-km resolution for the period January 1982–December 1993. The high spatial variation within these NDVI data emphasizes the significant differences in vegetation phenology across North America. For the purposes of this research, these Pathfinder NDVI data were aggregated from their original  $8\text{ km} \times 8\text{ km}$  pixel scale to the  $50\text{ km} \times 50\text{ km}$  fine-grid scale. An example NDVI distribution derived in this way for August 1989 is presented in Fig. 3a. The spatial pattern of NDVI shows a clear gradient from the southeast corner of the domain toward the northwest, which is consistent with the spatial distributions of temperature and precipitation. The time dependence of the domain-averaged NDVI for some of the most common vegetation classes

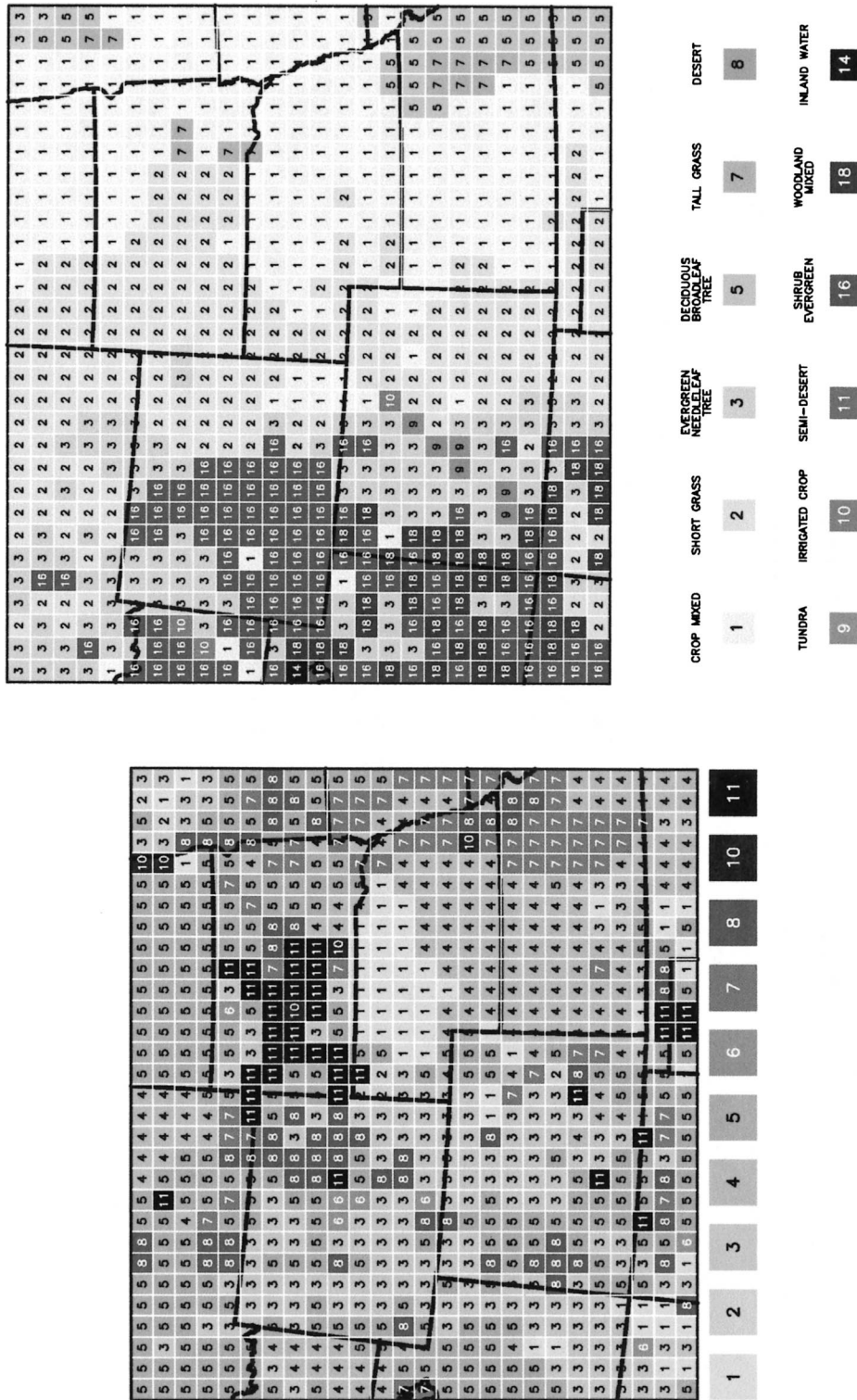


FIG. 2. (a) The soil-texture-class spatial distribution used in the fine grid defined from the USDA STATSGO database (Miller and White 1998). The numbers correspond to the following ClimRAMS soil classes: 1, sand; 2, loamy sand; 3, sandy loam; 4, silt loam; 5, loam; 6, sandy clay loam; 7, silty clay loam; 8, clay loam; 9, silty clay; 10, silty loam; 11, clay. Soil classes 9 (sandy peat) and 12 (peat) are not included in this domain at this resolution. (b) The distribution of vegetation classes used in the fine grid. The different vegetation classes are defined in the figure.

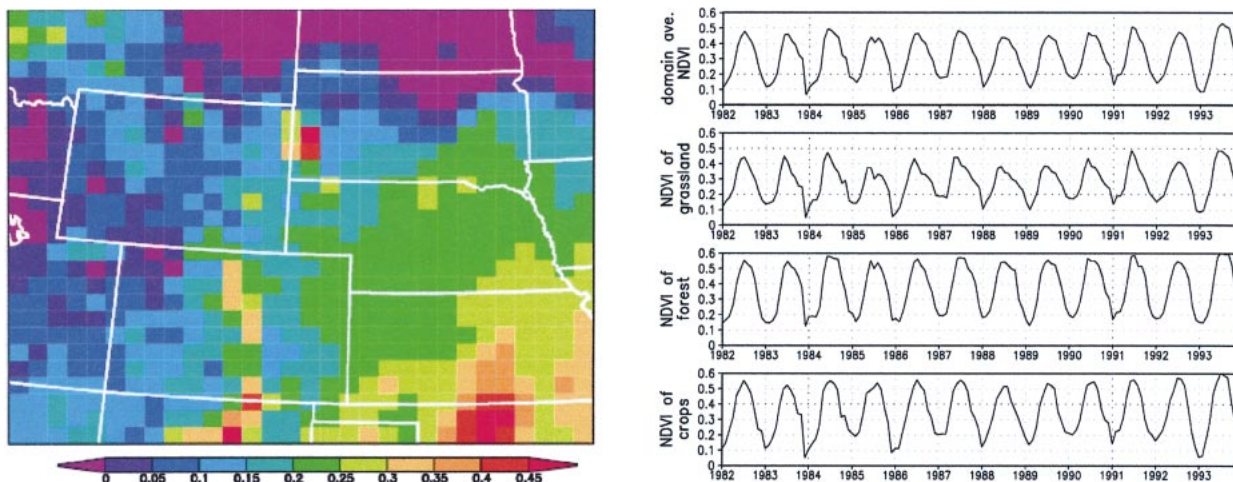


FIG. 3. (a) The spatial distribution of NDVI across the fine grid for Aug 1989 after aggregation from the 8-km pixel scale to the 50-km resolution. (b) Time series of monthly average NDVI for the period Jan 1982–Dec 1993 averaged over the domain of the fine grid for the more common vegetation types present.

within the area of the fine grid is displayed in Fig. 3b. The noticeable feature of the temporal profiles of NDVI over this simulation domain is its seasonality, with NDVI peaking during the months of June, July, and August and reaching a minimum (of around 0.1) during the winter. The domain-averaged NDVI time series for different vegetation types (Fig. 3b) have different amplitude, growing season length, and the residue after senescence, which can vary between years. The large interannual NDVI variability of grasslands contrasts with the limited variability of trees and crops, which is in line with expectation. The rapid growth in spring and early summer and prompt senescence in fall are also striking features of the central United States NDVI record.

#### b. Surface climate observations

Validating ClimRAMS and investigating the relationships between the vegetation growth cycle and climate requires a dataset of surface meteorological observations that has the spatial and temporal coverage for the domain and time span of interest. The first-order Summary of the Day (SOD) meteorological station observational data from the National Climatic Data Center (NCDC), which include observations of the daily precipitation, snowfall, snow depth, maximum screen-height air temperature ( $T_{\max}$ ), and minimum screen-height air temperature ( $T_{\min}$ ), are ideal for this purpose. The locations of 3800 SOD stations distributed across the United States are shown in Fig. 4a. Data from 1982 to 1996 were obtained and gridded onto the 50-km ClimRAMS grid using an objective analysis scheme following Cressman (1959). The monthly mean maximum and minimum screen-height air temperatures ( $T_{\max}$  and  $T_{\min}$ ) and precipitation, averaged over the domain of the fine grid for the period 1982–96, are given in Fig. 4b.

All three variables demonstrated consistent seasonal cycles. In this domain, the winter is dry and cold, while the summer is warm and receives most of the annual precipitation. Precipitation appears to have more interannual variability than temperature. The year 1989 was chosen as a near-average year for the control simulation of the model.

#### c. Correlation between vegetation index and atmospheric variables

The SOD and NDVI datasets exhibit some correlation. To illustrate this, the monthly, domain-averaged  $T_{\max}$ ,  $T_{\min}$ , precipitation, and NDVI values were averaged over June–July–August (JJA), that is, the peak growing season in Northern Hemisphere midlatitudes. The resulting time series are shown in Fig. 5. The following observations can be made:

- 1) The  $T_{\min}$  time series closely follows the  $T_{\max}$  time series, but the year-to-year variations are approximately twice as large for  $T_{\max}$ .
- 2) The temperatures and precipitation time series appear to be negatively correlated.
- 3) The domain-averaged NDVI time series resembles the domain-averaged precipitation time series, with the driest year (1988) having the lowest NDVI value and the wettest year (1993) having the highest.
- 4) The correlation coefficients between precipitation and domain-averaged NDVI, grasslands, trees, and crops are 0.65, 0.64, 0.42, and 0.76, respectively.

Thus, NDVI and rainfall in the central United States are positively correlated, reflecting the fact that vegetation growth depends strongly on soil-moisture availability, which in turn depends on rainfall amount and frequency. In part, this is also why the NDVI of grassland exhibits greater interannual variability than trees

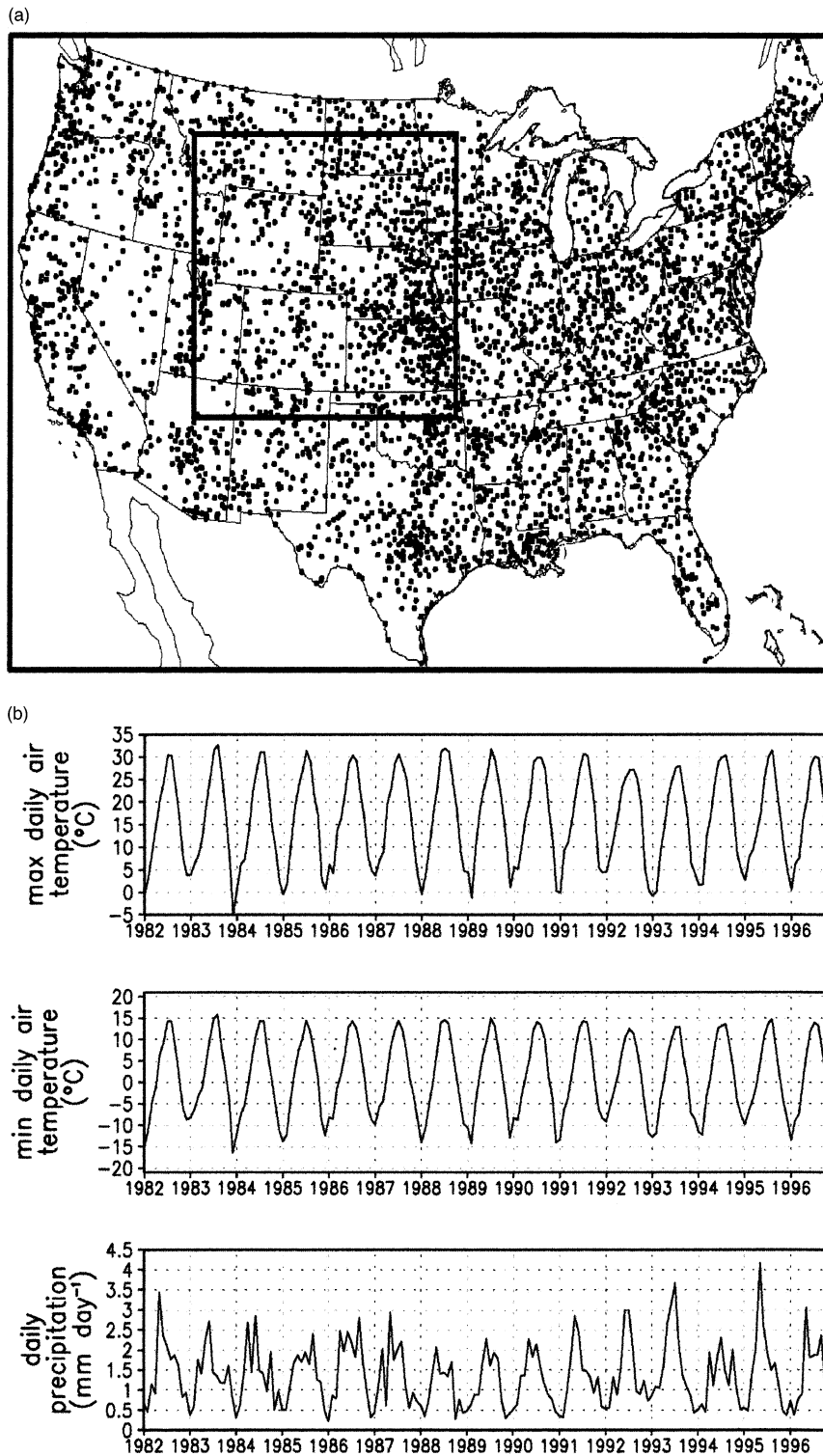


FIG. 4. (a) Locations of the stations in the NCDC Summary of the Day network, the data from which were used in this study. (b) Monthly average SOD observations of screen-height maximum and minimum air temperature and precipitation averaged over the domain of the fine grid for the period of 1982–96.

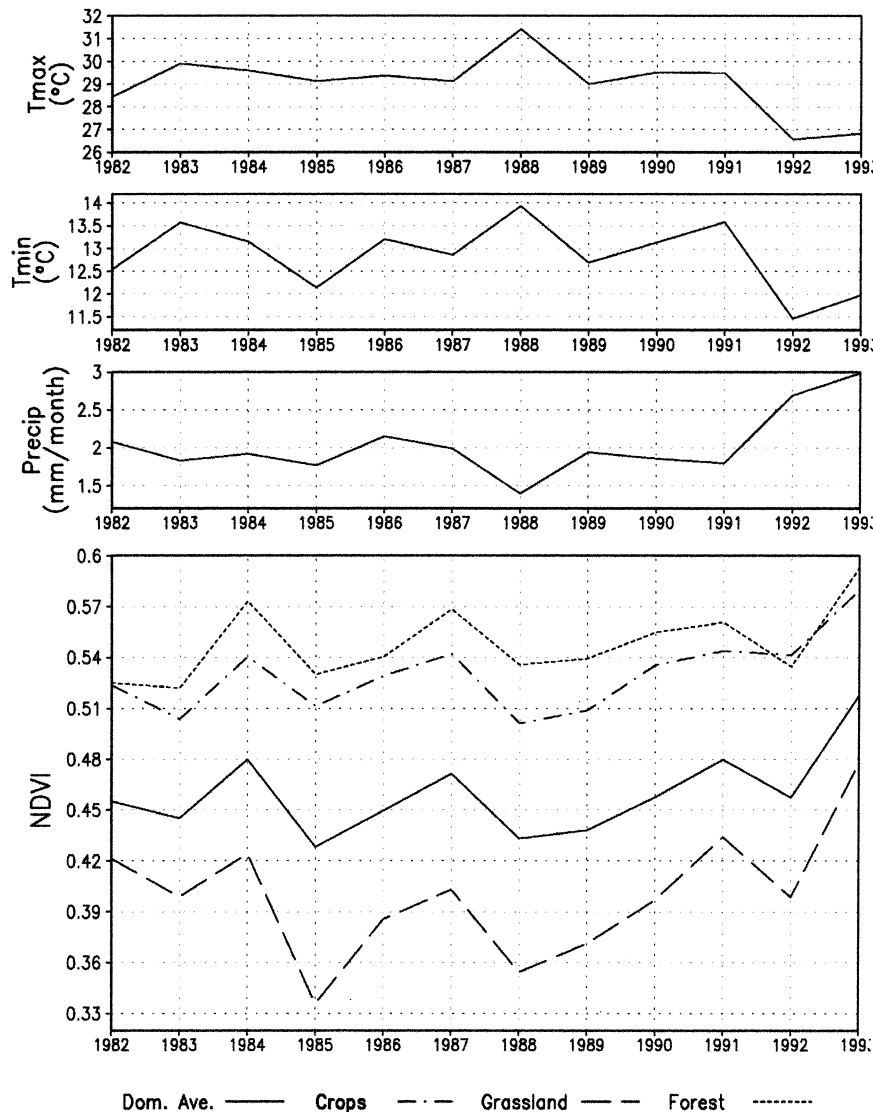


FIG. 5. Time series of climate variables and NDVI averaged over the domain of the fine grid for the period 1982–93. JJA average values, selected to represent the values during the peak growing season, are shown.

and crops: the deeper and more extensive rooting of trees and the irrigation of many crops may well allow them to have more consistent access to soil moisture than grasslands. The fact that NDVI and precipitation are significantly correlated argues for the use of realistic vegetation growth models in climate simulations. Figure 5 (bottom) shows that natural grasslands have the smallest value of NDVI, trees have the largest, and crops lie between the two.

#### d. NDVI-to-LAI conversion algorithm

Several algorithms exist to derive LAI from NDVI datasets (e.g., Sellers et al. 1996; Nemani et al. 1996). The algorithm introduced by Sellers et al. (1996) was

applied in this study as follows. First, a lookup table was created to relate the vegetation classes used in RAMS to those used in the second Simple Biosphere Model (SiB2) (Lu 1999; Lu et al. 2001). Then, the simple ratio SR was calculated, based on the relation  $SR = 1 + NDVI/1 - NDVI$ . The fractional photosynthetically active radiation (FPAR) is then given by

$$FPAR = \frac{(SR - SR_{i,min})(FPAR_{max} - FPAR_{min})}{(SR_{i,max} - SR_{i,min})} + FPAR_{min},$$

where  $FPAR_{max} = 0.950$ ,  $FPAR_{min} = 0.001$ ,  $FPAR_{max}$  and  $FPAR_{min}$  are independent of vegetation type,  $SR_{i,max}$  is equal to the SR value corresponding to 98% of the

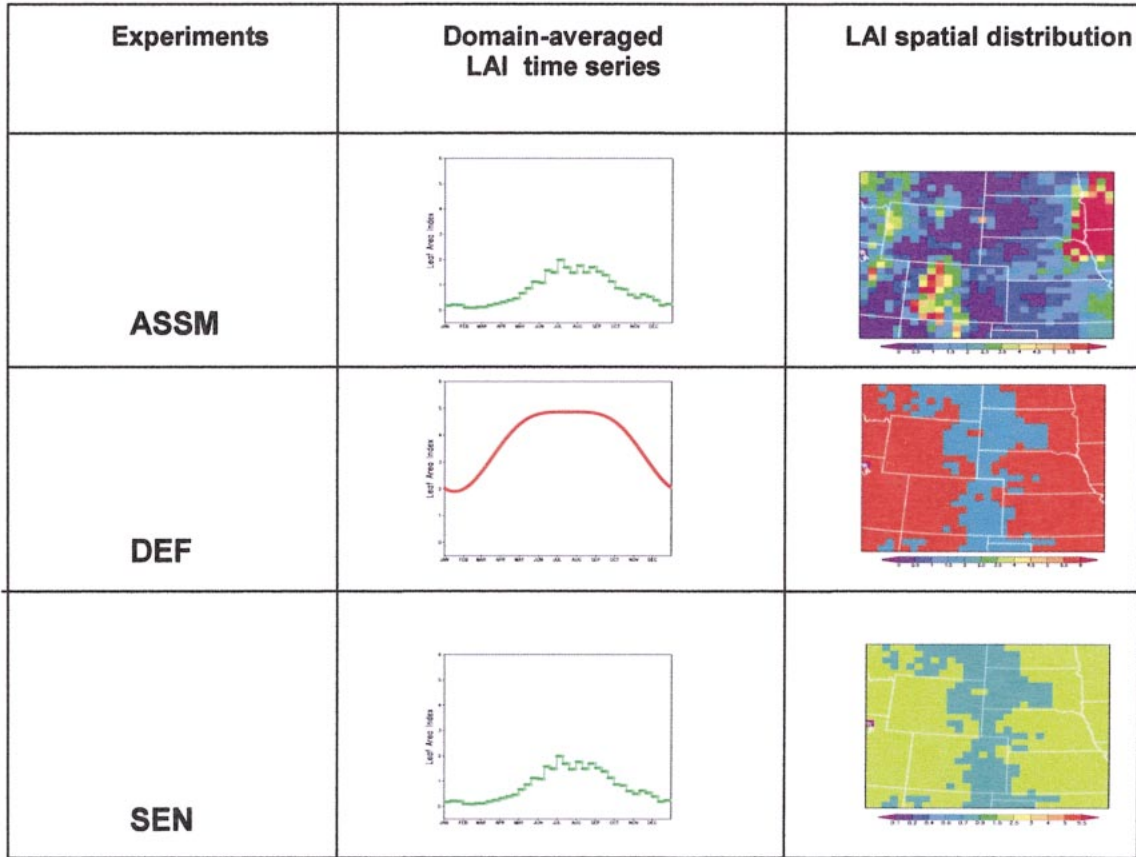


FIG. 6. Summary of the temporal and spatial distributions of LAI used in the three ClimRAM runs [ASSM (the run with assimilation of LAI derived from NDVI data), DEF (the run with the default specification of LAI for ClimRAMS), and SEN (the run in which the spatial distribution of LAI follows that in the DEF run)], but the values of LAI are all scaled down so that the domain-averaged value on each day is the same as for the ASSM run.

NDVI population  $i$ , and  $SR_{i,min}$  is equal to the SR value corresponding to 5% of the NDVI population.

It is assumed that the relationship between FPAR and the LAI for evenly distributed vegetation at a regional scale can be described by an exponential equation (Monteith and Unsworth 1990) with the form

$$LAI = LAI_{i,max} \frac{\log(1 - FPAR)}{\log(1 - FPAR_{max})},$$

where  $LAI_{i,max}$  is the maximum green leaf area index defined for vegetation type  $i$ . For clustered vegetation, for example, coniferous trees and shrubs, the equation becomes (Huemmrich and Goward 1992)

$$LAI = LAI_{i,max} \frac{FPAR}{FPAR_{i,max}}.$$

In cases where there is a combination of clustered and evenly distributed vegetation,

$$LAI = (1 - F_{cl})LAI_{i,max} \frac{\log(1 - FPAR)}{\log(1 - FPAR_{max})} + F_{cl} \frac{LAI_{i,max} FPAR}{FPAR_{max}},$$

where  $F_{cl}$  is the fraction of clumped vegetation in the grid area. The value of  $F_{cl}$  for each land-cover class can be found in Sellers et al. (1996).

#### 4. Experiment design and results

##### a. Experimental design

Three experiments were carried out to evaluate the impact of directly assimilating NDVI-derived estimates of LAI into ClimRAMS. In the first run, here called the “assimilation” (ASSM) run, the LAI is derived from the NDVI observations. In the second run, here called the “default” (DEF) run, LAI was prescribed to follow the standard used in ClimRAMS (which follows that of the equivalent BATS classes). The third run was a sensitivity test (SEN), in which the LAI has the same spatial distribution as for the DEF run, but the domain-averaged value of LAI (and each contributing LAI) was reduced to agree with the LAI derived from the NDVI observations. The spatial and temporal LAI distributions used in these three experiments are shown in Fig. 6.

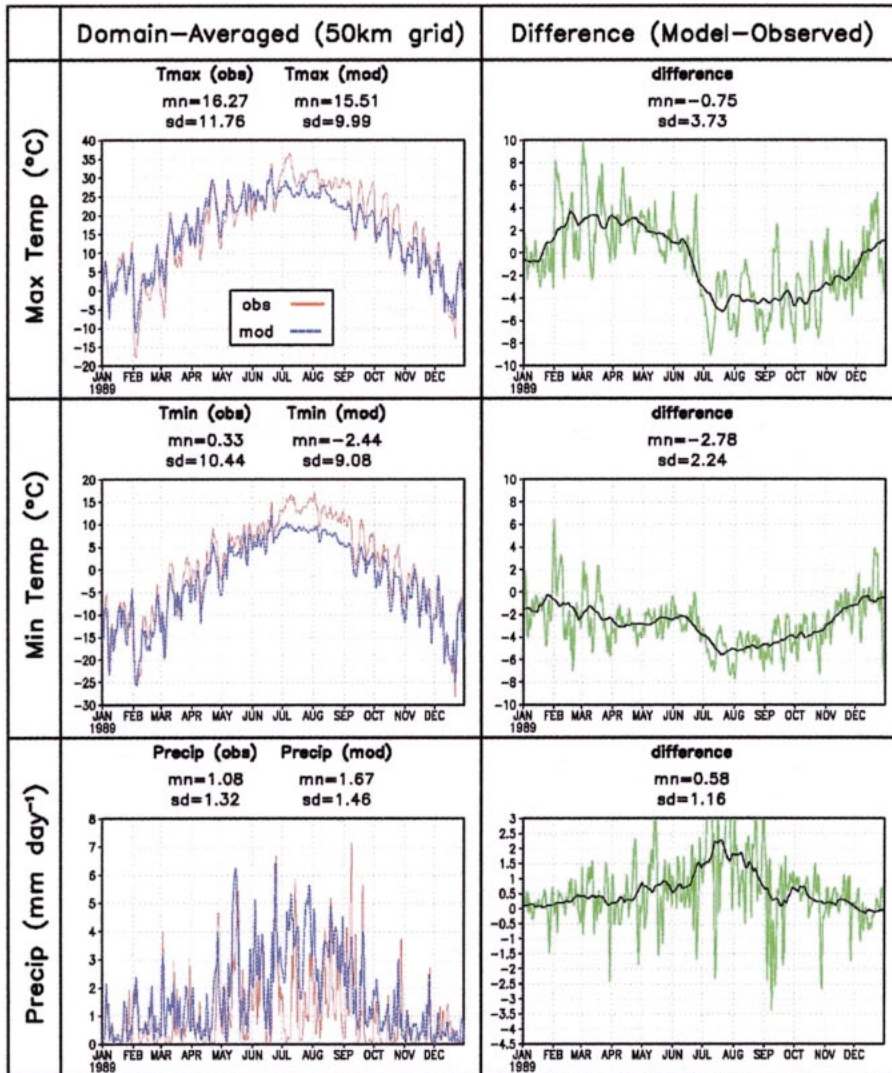


FIG. 7. Observed, domain-averaged daily maximum and minimum screen-height air temperature and daily precipitation for 1989 compared with the equivalent values calculated by ClimRAMS with assimilation of LAI derived from NDVI. The variables have all been averaged over the (50 km) fine grid. Also shown is the difference between the model and observations, and the 30-day running mean of these differences. The mean (mn) and standard deviation (sd) for each panel and variable are included.

*b. Results*

The primary purpose of the present study was to investigate the impact of assimilating observational vegetation information directly into ClimRAMS. Consequently, no attempt was made to “tune” model parameters in order to bring the ASSM simulation closer to observations, although this could easily have been done. (Note: because the soil-moisture initialization and coefficients in the precipitation parameterization used in ClimRAMS have already been adjusted to match the observations when the model is run in default mode, it is to be expected, in the absence of retuning, that the DEF run will give better agreement with the observed climate than the ASSM run.) The present analysis fo-

cuses on analyzing the differences between ASSM, DEF, and SEN simulations and what causes them. However, an initial check was made to ensure that the ASSM run was broadly consistent with observations as described below.

1) ASSIMILATION RUN COMPARED TO OBSERVATIONS

The simulated climate given by the ClimRAMS run in which NDVI was assimilated (ASSM) is summarized in Figs. 7 and 8. The model’s ability to reproduce the observed domain-averaged daily maximum ( $T_{max}$ ) and minimum ( $T_{min}$ ) screen-height air temperature and the

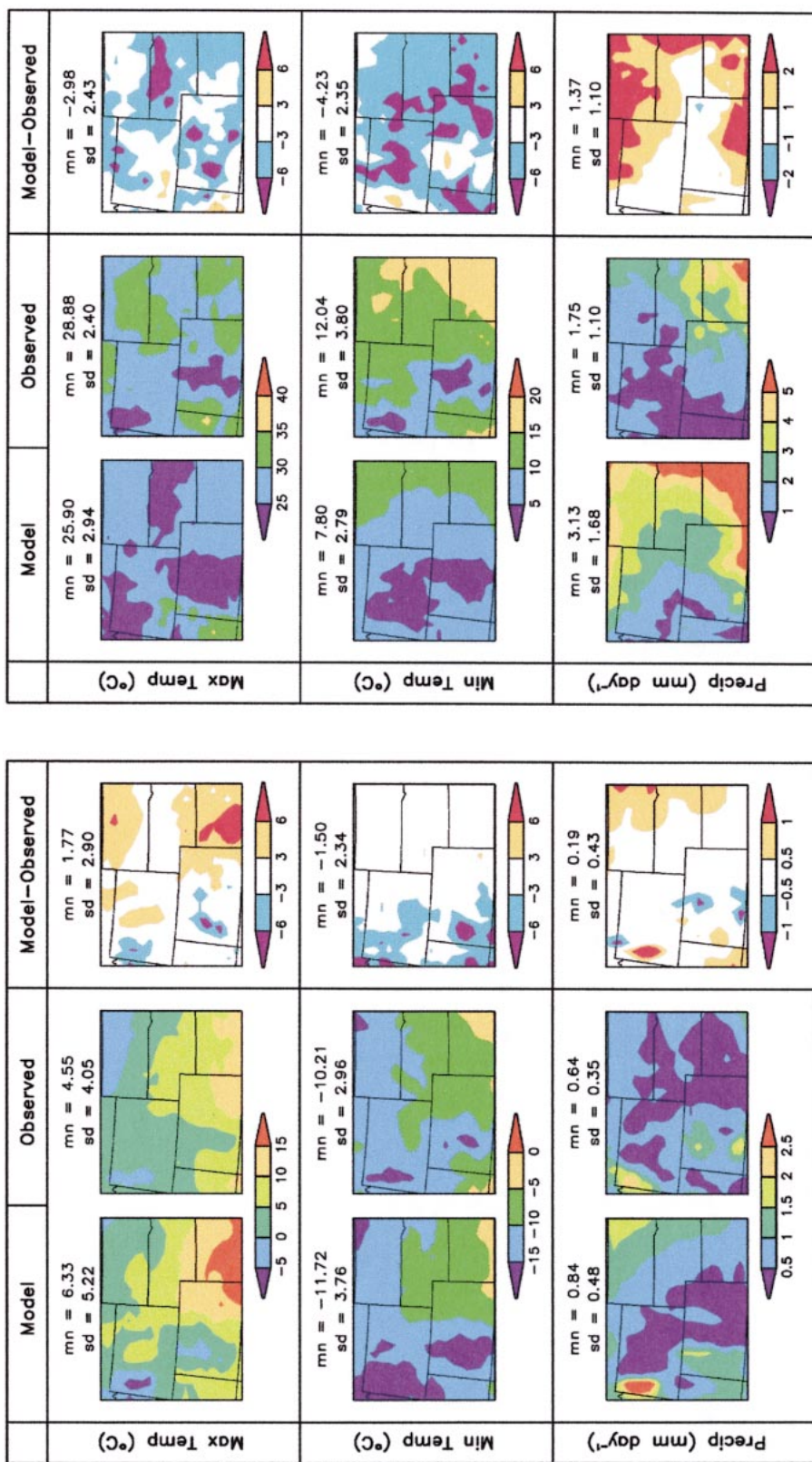


FIG. 8. Spatial patterns of maximum and minimum daily screen-height temperature and daily precipitation, averaged (a) Jan-Mar 1989, and (b) Jun-Aug 1989. Shown are the modeled fields given by ClimRAMS using NDVI-derived LAI and observed fields, and the differences between the two. The mean (mn) and standard deviation (sd) for each panel and variable are also given.

daily precipitation is presented in Fig. 7, these variables having been averaged over the domain of the nested, 50-km grid. The mean (mn) and standard deviation (sd) for each panel and variable are also given in Fig. 7. In each case, the difference between the modeled and observed values is also shown, together with a 30-day running mean of these differences. It is reassuring that the model simulation adequately captures the synoptic signal and evolution in seasonal temperature. Over the year, the model-simulated  $T_{\max}$  and  $T_{\min}$  are, on average,  $0.75^{\circ}$  and  $2.78^{\circ}\text{C}$  lower than observations, respectively, while the modeled daily precipitation is, on average,  $0.58\text{ mm day}^{-1}$  too high with respect to observations. The overestimation of precipitation occurs mainly in JJA, that is, during the growing season; consequently, the simulated Northern Hemisphere summer is colder and wetter than observations in this domain.

The spatial patterns of  $T_{\max}$ ,  $T_{\min}$ , and precipitation generally capture the observed spatial patterns during the winter months of January, February, and March (Fig. 8a) and the summer months June, July, and August (Fig. 8b). (Note: the temperature fields presented here have not been corrected for the elevation differences between the modeled values and observations.) A comparison of the annual cycle of  $T_{\max}$ ,  $T_{\min}$ , and daily precipitation at the model grid cell level, corresponding to three cities (Salina, Kansas; Sioux Falls, South Dakota; and Casper, Wyoming) within the fine-grid domain (not shown), confirm that the model is able to capture the regional differences in both temperature and precipitation at these locations. In summary, without retuning of model parameters, the ASSM model simulation, in general, successfully captured the seasonal variation in the primary atmospheric variables, although, undoubtedly, some tuning of model parameters could be made to further improve the model's diagnostic and forecasting skill.

## 2) ASSIMILATION RUN COMPARED TO DEFAULT RUN

The values of  $T_{\max}$ ,  $T_{\min}$ , and precipitation averaged over the fine grid given by the ASSM and DEF runs are given in Fig. 9a. The differences between values calculated in the ASSM and DEF simulations are also plotted, together with 30-day running mean of these differences. The value of  $T_{\max}$  given by the ASSM run is lower than that given by the DEF run from June through mid-October but is higher for the remainder of the year. The value of  $T_{\min}$  given by the ASSM run is colder than for the DEF run from April through November. Taken over the year, the ASSM run simulated  $T_{\max}$  and  $T_{\min}$  as being on average  $1.38^{\circ}\text{C}$  higher and  $0.91^{\circ}\text{C}$  lower, respectively, than the DEF run. The daily precipitation simulated by the ASSM run is on average  $0.68\text{ mm day}^{-1}$  more than for the DEF run, which is the main reason why the modeled climate in the ASSM run is generally colder than in the DEF run during the

growing season, when the additional precipitation mainly occurs.

The differences between the LAI distributions used in the ASSM and DEF are clearly apparent in Fig. 6. In the DEF run, seasonal evolution of LAI is defined by the BATS classification and has a sinusoidal variation with the day of the year. Consequently, the spatial pattern and, indeed, magnitude of the LAI stay much the same from June through October. On the other hand, the ASSM run uses the 10-day composite NDVI data to derive the specification of LAI, which results in much greater heterogeneities across the modeled domain, both in terms of the spatial distribution and the seasonal evolution of the LAI. It is well known that such land surface heterogeneity can induce mesoscale circulations in the atmosphere that not only influence the surface layer immediately above the vegetation, but which also can trigger moist convection and precipitation in preferred areas.

## 3) SENSITIVITY RUN COMPARED TO DEFAULT RUN

There are two striking differences between the specification of LAI used in the ASSM and DEF runs. First, the magnitude of the domain-averaged LAI during the summer season is approximately a factor of 2 less for the ASSM run than for the DEF run. Second, the LAI spatial distribution of the LAI used in the ASSM run is much more heterogeneous than that used in the DEF run. The question arises: Which factor leads to the extra precipitation produced during the ASSM run? To clarify this issue, a third run (SEN) was carried out in which the LAI was specified to have the same domain-averaged value as the ASSM run, but the spatial distribution of the DEF run (Fig. 6). Specifically, the LAI for each default vegetation class was scaled down by a factor equal to the ratio of the domain-averaged LAI for the ASSM run divided by the domain-averaged LAI for the DEF run, this latter ratio being, of course, a function of the day of the year. Comparison between the simulated climates given in the SEN and ASSM runs relative to that given by the DEF run should define whether it is the overall magnitude of the NDVI-derived LAI or greater LAI heterogeneity that is most important.

The domain-averaged values of  $T_{\max}$ ,  $T_{\min}$ , and daily precipitation for the SEN and DEF runs are shown in Fig. 9b, together with differences between these variables, and 30-day running mean of these differences. There is a marked difference between Figs. 9a and 9b. The climate simulated by the SEN run much more closely follows that simulated by the DEF run. On average, for 1989, the values of  $T_{\max}$  and  $T_{\min}$  by the SEN run are  $1.32^{\circ}\text{C}$  higher and  $0.92^{\circ}\text{C}$  lower, respectively, than those simulated by the DEF run, and the precipitation is on average  $0.06\text{ mm day}^{-1}$  lower than for the DEF run during the growing season. Thus, the climate simulated in the SEN run, in fact, has a drier and warmer summer than the DEF run, the opposite result to that

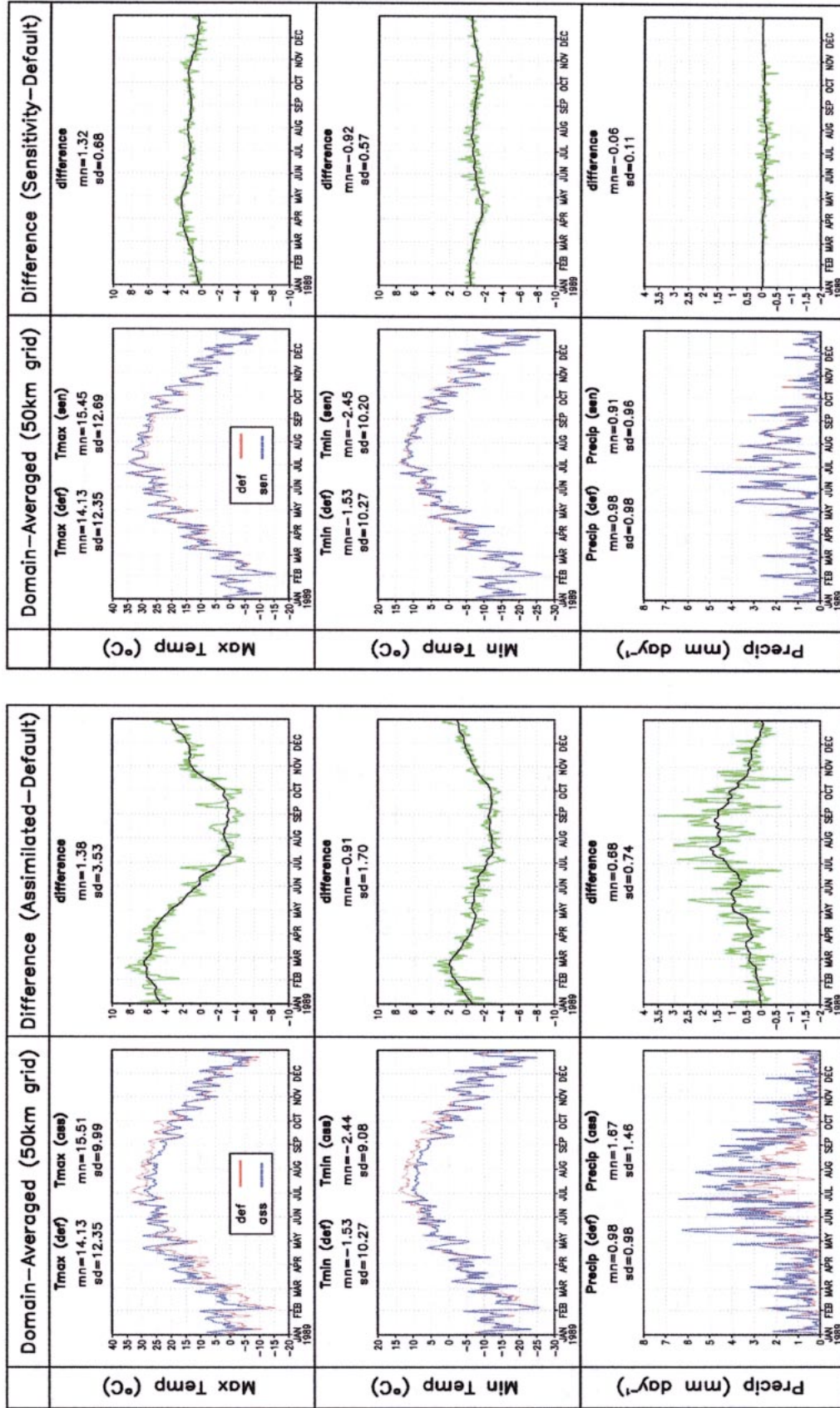


FIG. 9. Domain-averaged daily maximum and minimum screen-height air temperature and daily precipitation for 1989 calculated by ClimRAMS for (a) the DEF and ASSM runs, and (b) the SEN and DEF runs. In each case, the variables have all been averaged over the (50 km) fine grid. Also shown is the difference between the model and observations, and the 30-day running mean of these differences. The mean (mn) and standard deviation (sd) for each panel and variable are included.

for the ASSM run. Consequently, reducing the magnitude of LAI alone does not contribute to the extra precipitation simulated in the ASSM run. On the contrary, the simulated precipitation decreased (as might be expected if the overall magnitude of the LAI decreases). We conclude that it is the introduction of heterogeneity into NDVI-derived fields that is the primary cause of the generally wetter and colder summer climate produced in the ASSM simulation.

This is an important result. Assuming that ClimRAMS is typical of other regional climate models, this suggests that when climate is simulated with a model that has a grid mesh sufficiently fine for the effect of surface heterogeneities to have impact on modeled convective processes, not only the temporal but also the spatial distribution of LAI can have a significant impact on the simulated area-average climate. However, because this result may be model- and domain-dependent, it is important that it is tested with other models at other locations.

## 5. Summary, discussion, and conclusions

This study focused on implementing the assimilation of NDVI-derived LAI into ClimRAMS and evaluating the impact of doing so on the climate simulated by the model. Our results show that the regional climate modeled by ClimRAMS with assimilation of NDVI remains reasonable relative to observations without any attempt to tune the model from its default state. We also found the modeled climate to be sensitive to the specification of LAI in fact have a first-order effect on the modeled weather and climate. When NDVI-derived LAI is assimilated, the modeled climate is cooler and has more precipitation than that simulated by ClimRAMS using its default LAI specification. Further, the effect of heterogeneity in LAI (when combined with a reduced magnitude of LAI) appears to dominate over the effect of an overall area-average reduction in LAI acting alone. Our primary conclusion is, therefore, that including a realistic description of the phenology of heterogeneous vegetation can and, at least in the case of ClimRAMS, does influence the prediction of seasonal climate in a regional climate model that has sufficient resolution to resolve some of the surface heterogeneity in LAI.

Four-Dimensional Data Assimilation (4DDA) is widely used as the basis of initiating real-time weather forecasts, and the required real-time global network for atmospheric observation is well established. The recent advent of land surface information derived from satellite observations opens up the possibility of assimilating new variables, such as leaf area index (LAI), surface albedo, and soil moisture into numerical models. This study suggests that there may be potential benefit in assimilating at least indirectly measured LAI in real-time into regional models.

While conducting our sensitivity experiments with a coupled modeling system, we realize that regional atmospheric models are necessarily highly constrained by their prescribed lateral boundary conditions, and some of the effect of vegetation feedback may be lost. Land surface properties can act as a mechanism to provide “triggering effects” in regional climate models, with the overall water and energy budget still largely prescribed by boundary conditions, and the effect of land surface characteristics being mainly a redistribution of water and energy within the simulation domain. In the present study, this was mitigated by two-way nesting of the high-resolution domain of interest within a much larger domain, but some remnant influences of boundary forcing may still be present in our results.

Overall, our study makes a case for the real-time use of satellite-derived LAI in fine-resolution climate models, preferably in fine-resolution climate models operating at a global scale, but at least in fine-resolution regional climate models that are two-way nested within general circulation models. Associated with this is the continuing need for improved NDVI data retrieval processes and the NDVI-to-LAI conversion algorithms. Fortunately, this need is now receiving increased attention with the advent of relevant satellite systems within the Earth Observing System. There is also a continuing need to advance high-resolution global-scale modeling capability. A parallel programming version of ClimRAMS is currently being developed that can run at higher resolution for several years. Hopefully, this new modeling system will be able to resolve mesoscale circulations generated by land surface heterogeneities—an important feature in the present study—and at the same time represent the possible long-term feedbacks from the vegetation and soil moisture. Thus, on the basis of this study, we argue that assimilating the observed vegetation distribution into models is worthwhile, and we anticipate that including remotely sensed observations of vegetation cover will soon become standard in 4DDA systems.

*Acknowledgments.* The research described in this paper was carried out in support of the GCIP/GAPP program, with primary support provided under NASA Grant NAG8-1531. The present study was greatly facilitated by the ready availability of datasets that were originally prepared for an earlier study while Dr. Lu was a graduate research assistant at Colorado State University. The guidance and support of Drs. R. A. Pielke Sr., G. E. Liston, and S. A. Denning during that doctoral program are greatly appreciated.

## REFERENCES

- Arakawa, A., and R. V. Lamb, 1977: Computational design of the basic dynamical processes of the UCLA general circulation model. *Methods in Computational Physics*, Vol. 17. Academic Press, 174–265.
- Avissar, R., and Y. Mahrer, 1988: Mapping frost-sensitive areas with

- a three-dimensional local-scale numerical model. Part I: Physical and numerical aspects. *J. Appl. Meteor.*, **27**, 400–413.
- , P. Avissar, Y. Mahrer, and B. A. Bravdo, 1985: A model to simulate response of plant stomata to environmental conditions. *Agric. For. Meteorol.*, **34**, 21–29.
- Bonan, G. B., 1997: Effects of land use on the climate of the United States. *Climatic Change*, **37**, 449–486.
- Bounoua, L., G. J. Gollatz, S. O. Los, P. J. Sellers, D. A. Dazlich, C. J. Tucker, and D. A. Randall, 2000: Sensitivity of climate to changes in NDVI. *J. Climate*, **13**, 2277–2292.
- Charney, J. G., 1975: Dynamics of deserts and drought in the Sahel. *Quart. J. Roy. Meteor. Soc.*, **101**, 193–202.
- , W. J. Quirk, S. H. Chow, and J. Kornfield, 1977: A comparative study of the effects of albedo change on drought in semi-arid regions. *J. Atmos. Sci.*, **34**, 1366–1385.
- Chase, T. N., R. A. Pielke, T. G. F. Kittel, R. Nemani, and S. W. Running, 1996: The sensitivity of a general circulation model to global changes in leaf area index. *J. Geophys. Res.*, **101**, 7393–7408.
- , —, —, —, and —, 2000: Simulated impacts of historical land cover changes on global climate in northern winter. *Climate Dyn.*, **16**, 93–105.
- Clapp, R., and G. Hornberger, 1978: Empirical equations for some soil hydraulic properties. *Water Resour. Res.*, **14**, 601–604.
- Clark, T. L., 1977: A small-scale dynamic model using a terrain-following coordinate transformation. *J. Comput. Phys.*, **24**, 186–215.
- Claussen, M., 1994: On coupling global biome models with climate models. *Climate Res.*, **4**, 203–221.
- , 1998: On multiple solutions of the atmosphere–vegetation system in present-day climate. *Global Change Biol.*, **4**, 549–559.
- , V. Brovkin, A. Ganopolski, C. Kubatzki, and V. Petoukhov, 1998: Modeling global terrestrial vegetation–climate interaction. *Philos. Trans. Roy. Soc. London*, **353B**, 53–63.
- Copeland, J. H., R. A. Pielke, and T. G. F. Kittel, 1996: Potential climatic impacts of vegetation change: A regional modeling study. *J. Geophys. Res.*, **101**, 7409–7418.
- Cotton, W. R., J. F. Weaver, and B. A. Beitler, 1995: An unusual summertime downslope wind event in Fort Collins, Colorado, on 3 July 1993. *Wea. Forecasting*, **10**, 786–797.
- Cressman, G. P., 1959: An operational objective analysis system. *Mon. Wea. Rev.*, **87**, 367–374.
- Deardorff, J. W., 1978: Efficient prediction of ground surface temperature and moisture, with inclusion of layer of vegetation. *J. Geophys. Res.*, **83**, 1889–1903.
- Dickinson, R. E., J. Jaeger, W. M. Washington, and R. Wolski, 1981: Boundary subroutine for the NCAR global climate model. NCAR Tech. Note 173+1A, 75 pp.
- , A. Henderson-Sellers, P. J. Kennedy, and M. F. Wilson, 1986: Biosphere–Atmosphere Transfer Scheme (BATS) for the NCAR community climate model. Tech. Note NCAR/TN-275+STR, 69 pp.
- , —, and —, 1993: Biosphere–Atmosphere Transfer Scheme (BATS) version 1e as coupled to the NCAR community climate model. Tech. Note NCAR/TN-378+STR, 72 pp.
- , M. Shaikh, R. Bryant, and L. Graumlich, 1998: Interactive canopies for a climate model. *J. Climate*, **11**, 2823–2836.
- Dirmeyer, P. A., 1994: Vegetation stress as a feedback mechanism in midlatitude drought. *J. Climate*, **7**, 1463–1483.
- Farouki, O. T., 1986: *Thermal Properties of Soils*, Series on Rock and Soil Mechanics, Vol. 11, Enfield, 1–136.
- Foley, J. A., 1994: The sensitivity of the terrestrial biosphere to climate change: A simulation of the middle Holocene. *Global Biogeochem. Cycles*, **8**, 505–525.
- Gash, J. H. C., and C. A. Nobre, 1997: Climatic effects of Amazonian deforestation: Some results from ABRACOS. *Bull. Amer. Meteor. Soc.*, **78**, 823–830.
- Huemmerich, K. F., and S. N. Goward, 1992: Spectral vegetation indexes and the remote sensing of biophysical parameters. *Proc. Int. Geoscience and Remote Sensing Symp. (IGARSS)*, Houston, TX, Institute of Electrical and Electronics Engineers, 1017–1019.
- Kalnay, E., and Coauthors, 1996: The NCEP/NCAR 40-Year Reanalysis Project. *Bull. Amer. Meteor. Soc.*, **77**, 437–471.
- Koster, R., J. Jouawil, R. Suozzo, and G. Russel, 1986: Global sources of local precipitation as determined by the NASA/GISS GCM. *Geophys. Res. Lett.*, **13**, 121–124.
- Lee, T. J., 1992: The impact of vegetation on the atmospheric boundary layer and convective storms. Ph.D. dissertation, Dept. of Atmospheric Science Paper 509, Colorado State University, 137 pp.
- Liston, G. E., and R. A. Pielke, 2000: A climate version of the Regional Atmospheric Modeling System. *Theor. Appl. Climatol.*, **66**, 29–47.
- Louis, J. F., 1979: A parametric model of vertical eddy fluxes in the atmosphere. *Bound.-Layer Meteorol.*, **17**, 187–202.
- , M. Tiedtke, and J. F. Geleyn, 1982: A short history of the PBL parameterization at ECMWF. *Proc. 1981 Workshop on PBL Parameterization*, Shinfield Park, Reading, United Kingdom, ECMWF, 59–71.
- Lu, L., 1999: Implementation of a two-way interactive atmospheric and ecological model and its application to the central United States. Ph.D. dissertation, Dept. of Atmospheric Science, Colorado State University, 134 pp.
- , R. A. Pielke, G. E. Liston, W. J. Parton, D. Ojima, and M. Hartman, 2001: Implementation of a two-way interactive atmospheric and ecological model and its application to the central United States. *J. Climate*, **14**, 900–919.
- McCumber, M. C., and R. A. Pielke, 1981: Simulation of the effects of surface fluxes of heat and moisture in a mesoscale numerical model, Part I: Soil layer. *J. Geophys. Res.*, **86**, 9929–9938.
- Meehl, G. A., and W. M. Washington, 1988: Comparison of soil moisture sensitivity in two global climate models. *J. Atmos. Sci.*, **45**, 1476–1492.
- Miller, D. A., and R. A. White, 1998: A conterminous United States multilayer soil characteristics dataset for regional climate and hydrology modeling. *Earth Interactions*, **2**. [Available online at <http://EarthInteractions.org>.]
- Monteith, J. L., and M. H. Unsworth, 1990: *Principles of Environmental Physics*. Edward Arnold, 291 pp.
- Nemani, R. R., S. W. Running, R. A. Pielke, and T. N. Chase, 1996: Global vegetation cover changes from coarse resolution satellite data. *J. Geophys. Res.*, **101** (D3), 7157–7162.
- Oleson, K. W., and G. B. Bonan, 2000: The effects of remotely sensed plant functional type and leaf area index on simulations of boreal forest surface fluxes by the NCAR land surface model. *J. Hydrometeorol.*, **1**, 431–446.
- , W. J. Emery, and J. A. Maskanik, 2000: Evaluating land surface parameters in the Biosphere–Atmosphere Transfer Scheme using remotely sensed data sets. *J. Geophys. Res.*, **105**, 7275–7293.
- Pielke, R. A., and Coauthors, 1992: A comprehensive meteorological modeling system—RAMS. *Meteor. Atmos. Phys.*, **49**, 69–91.
- , T. J. Lee, J. H. Copeland, J. L. Eastman, C. L. Ziegler, and C. A. Finley, 1997: Use of USGS-provided data to improve weather and climate simulations. *Ecol. Appl.*, **7**, 3–21.
- , G. E. Liston, J. L. Eastman, L. Lu, and M. Coughenour, 1999: Seasonal weather prediction as an initial value problem. *J. Geophys. Res.*, **104**, 19 463–19 479.
- Rabin, R. M., S. Stadler, P. J. Wetzler, D. J. Stensrud, and M. Gregory, 1990: Observed effects of landscape variability on convective clouds. *Bull. Amer. Meteor. Soc.*, **71**, 272–280.
- Rhea, J. O., 1978: Orographic precipitation model for hydrometeorological use. Ph.D. dissertation, Dept. of Atmospheric Science Paper 287, Colorado State University, 199 pp.
- Segal, M., 1989: Impact of crop areas in northeast Colorado on mid-summer mesoscale thermal circulations. *Mon. Wea. Rev.*, **117**, 809–825.
- Sellers, P. J., S. O. Los, C. J. Tucker, C. O. Justice, D. A. Dazlich, G. J. Collatz, and D. A. Randall, 1996: A revised land surface parameterization (SiB2) for atmospheric GCMs. Part II: The

- generation of global fields of terrestrial biophysical parameters from satellite data. *J. Climate*, **9**, 706–737.
- Sepaskhah, A. R., and L. Boersma, 1979: Thermal conductivity of soils as a function of temperature and water content. *Soil Sci. Soc. Amer. J.*, **43**, 439–444.
- Shukla, J., and Y. Mintz, 1982: Influence of land-surface evapotranspiration on the earth's climate. *Science*, **215**, 1498–1501.
- Sud, Y. C., and W. E. Smith, 1985: Influence of surface roughness of deserts on the July circulation. *Bound.-Layer Meteor.*, **33**, 15–49.
- Texier, D., and Coauthors, 1997: Quantifying the role of biosphere-atmosphere feedbacks in climate change: Coupled model simulations for 6000 years BP and comparison with paleodata for northern Eurasia and northern Africa. *Climate Dyn.*, **13**, 865–882.
- Thompson, G., 1993: Numerical simulation of a mesoscale prediction during 1991–92 winter season and statistical verification of model data. M.S. thesis, Dept. of Atmospheric Science, Colorado State University, 105 pp.
- Tremback, C. J., 1990: Numerical simulation of a mesoscale convective complex: Model development and numerical results. Ph.D. dissertation, Dept. of Atmospheric Science Paper 465, Colorado State University, 247 pp.
- , and R. Kessler, 1985: A surface temperature and moisture parameterization for use in mesoscale numerical models. Preprints, *Seventh Conf. on Numerical Weather Prediction*, Montreal, PQ, Canada, Amer. Meteor. Soc., 355–358.
- Tripoli, G. J., and W. R. Cotton, 1980: A numerical investigation of several factors contributing to the observed variable intensity of deep convection over south Florida. *J. Appl. Meteor.*, **19**, 1037–1063.
- , and ———, 1982: The Colorado State University three-dimensional cloud/mesoscale model—1982, Part I: General theoretical framework and sensitivity experiments. *J. Rech. Atmos.*, **16**, 185–220.
- Xue, Y., 1997: Biosphere feedback on regional climate in tropical north Africa. *Quart. J. Roy. Meteor. Soc.*, **123**, 1483–1515.
- , M. J. Fennessy, and P. J. Sellers, 1996: Impact of vegetation properties on U.S. summer weather prediction. *J. Geophys. Res.*, **101**, 7419–7430.